LA-UR-13-21481
Approved for public release; distribution is unlimited.

Title: Slitting Method Measurement of Residual Stress Profiles, Including Stress Discontinuities, in Layered Specimens

Author(s): Prime, Michael B.
Crane, David L.

Intended for: SEM 2013 Annual Conference & Exposition on Experimental and Applied Mechanics, 2013-06-03/2013-06-05 (Lombard, Illinois, United States)

Final reference:

Prime, M. B., and Crane, D. L., 2014, "Slitting Method Measurement of Residual Stress Profiles, Including Stress Discontinuities, in Layered Specimens," Residual Stress, Thermomechanics & Infrared Imaging, Hybrid Techniques and Inverse Problems, Volume 8, Conference Proceedings of the Society for Experimental Mechanics Series, M. Rossi, M. Sasso, N. Connesson, R. Singh, A. DeWald, D. Backman, and P. Gloeckner, eds., Springer International Publishing, pp. 93-102.

Slitting Method Measurement of Residual Stress Profiles, Including Stress Discontinuities, in Layered Specimens

Michael B. Prime, David L. Crane
Los Alamos National Laboratory, P.O. Box 1663, Los Alamos, NM 87545

ABSTRACT

Layered specimens can, and often do, have discontinuities in residual stress across the material interfaces. Stress discontinuities internal to specimens are notoriously difficult to measure, yet they can have profound impact on debonding and other failures. The incremental slitting method, also known as crack compliance, is generally excellent at resolving stress profiles even when there are high gradients. However, the data reduction for slitting usually involves some smoothing, which makes it hard to resolve discontinuities. In this work, we start with a recent technique to analyze slitting data using Tikhonov regularization, and extend that technique to allow stress discontinuities at material interfaces. The new method is then demonstrated experimentally on several specimens, including metals and ceramics.

Keywords: residual stress, slitting, regularization, layers, inverse solution

INTRODUCTION

Residual stresses play a significant role in many material failure processes like fatigue, fracture, and stress corrosion cracking [1,2]. Residual stresses are the stresses present in a part free from external load, and they are generated by virtually any manufacturing process. The subject of this study is the measurement of residual stresses in layered specimens using the incremental slitting method [3,4].

Incremental slitting generally provides excellent spatial resolution of residual stress profiles [5-8], but accurate resolution of the discontinuous stress profile across layers is more challenging. Analyzing slitting data requires the solution of an elastic inverse problem to calculate the original residual stresses based on strains measured during the incremental deepening of a slit. Because the inverse solution tends to amplify noise in the strain data into larger noise in the stress profile, some type of smoothing is usually used. However, such smoothing makes it difficult to resolve discontinuities. In fact, the most common method for solving the inverse problem is to expand the stresses in terms of a continuous polynomial series [3,9], which does not allow for discontinuities at all. More sophisticated implementations of the series expansion method use piece-wise polynomials [10] which can resolve discontinuous stress profiles [11-13]. However, using piecewise polynomials is computationally intensive and numerically awkward.

In this work, we start with an inverse methodology that uses pulse functions and Tikhonov regularization [14] and has proven to be superior to the series expansion method for resolving stress profiles with high gradients [5,15]. A simple modification of the pulse-regularization approach allows one to resolve discontinuities while still retaining the regularization benefits of smoothing other portions of the stress profile. The method is demonstrated on several examples.

THEORY

Standard pulse-regularization

We first review the derivation of the traditional pulse-regularization method, for which the reader is referred to [14] for greater details, before moving onto the formulation that allows for discontinuities. Before adding regularization, the pulse method is equivalent to the “integral method,” long used for hole drilling [16]. Prior to inverting the equation to solve for stress, the pulse method is given in equation form by

$$\mathbf{G}\,\boldsymbol{\sigma} = \mathbf{d} \qquad (1)$$

Where **d** is a column vector of the strains measured at each slit depth and $\boldsymbol{\sigma}$ is a column vector of the stresses originally present over each increment of slit depth. **G** is a lower triangular matrix of the coefficients relating those stresses to the measured strains, as illustrated in Figure 1. The coefficients are usually determined using an elastic finite element analysis.

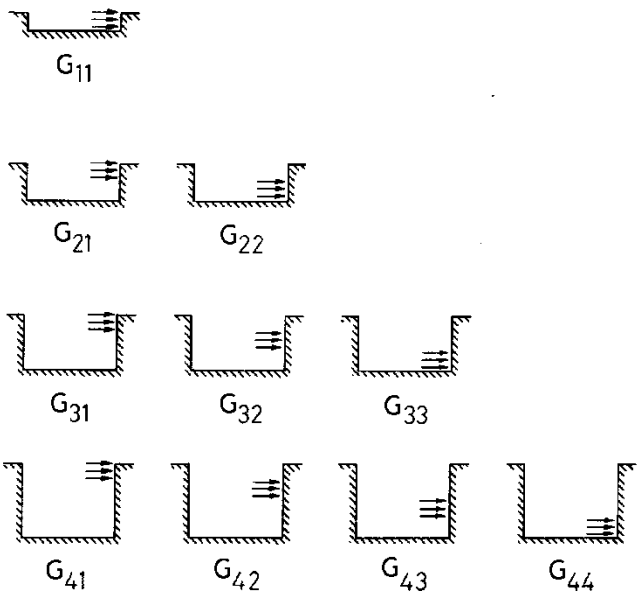

Figure 1. The coefficients G_{ij} correspond to the contribution of the stress over depth increment *j* to the strains measured at slit depth *i*. From [14].

For an equal number of stresses and strains, inverting Eq. 1 returns a stress vector that exactly reproduces the measured strains but generally results in a noisy solution and the undesired behavior that taking more data (meaning more depth increments) results in a noisier solution. For solutions using pulse functions without regularization, the noise amplification is usually kept small by using only a few unevenly spaced material removal increments. This approach is effective, but it diminishes the data content of the calculation, and decreases the spatial resolution of the stress solution.

Tikhonov regularization applies a penalty function to some measure of noise in the calculated stress profile. This procedure effectively smooths the stress solution. It diminishes the adverse effect of the noise without significantly distorting the part of the stress solution corresponding to the "true data". When implementing Tikhonov regularization, Equation (1) is pre-multiplied by $\mathbf{G}^T$ and augmented by an extra term. The result is:

$$(\mathbf{G}^T\mathbf{G} + \beta\,\mathbf{C}^T\mathbf{S}^T\mathbf{H}\,\mathbf{S}\,\mathbf{C})\,\boldsymbol{\sigma} = \mathbf{G}^T\mathbf{d} \qquad (2)$$

where the regularization comes from the matrix **C** which numerically approximates the second derivative of the stress profile. For evenly spaced data, **C** contains rows (-1,2,-1) centered along its main diagonal. For uniformly spaced data[1], the matrix product **H S C** has the following structure (for simplicity, illustrated for 4 cut increments)

$$\mathbf{H}\,\mathbf{S}\,\mathbf{C} = \begin{bmatrix} (h_1 - h_0)/W & & & \\ & (h_2 - h_1)/W & & \\ & & (h_3 - h_2)/W & \\ & & & (h_4 - h_3)/W \end{bmatrix} \begin{bmatrix} s_1 & & & \\ & s_2 & & \\ & & s_3 & \\ & & & s_4 \end{bmatrix} \begin{bmatrix} 0 & 0 & 0 & 0 \\ -1 & 2 & -1 & 0 \\ 0 & -1 & 2 & -1 \\ 0 & 0 & 0 & 0 \end{bmatrix} \qquad (3)$$

[1] See [14] for general formulas for unevenly spaced intervals

where the first and last rows of **C** are set to zero to eliminate the degenerate regularization that an "incomplete" (-1 2 -1) pattern would produce at the end points. *W* is the part thickness in the cutting direction, h_i is the slit depth at increment *i* and matrix **S** in Equations (2) and (3) contains along its main diagonal the standard errors s_i in the deformation data d_i.

In Equation (2), β is a weighting factor called the regularization parameter. β = 0 indicates no regularization, and β > 0 indicates an increasing amount of regularization. The Morozov Discrepancy Principle [17] can be used to determine the value of β that gives the optimal regularization that substantially reduces noise without significantly distorting the true solution. Equation 2 can be solved for stress using basic matrix algebra operations.

Pulse-regularization for layers and discontinuous stresses

Adapting the regularization approach to allow for discontinuities at known locations is as simple as removing select rows in the **C** matrix. For any given discontinuity that is directly at the interface between two depth increments, there are two rows in **C** that act to smooth across the interface that should be removed. An example of such a modified matrix for an example with 8 cut increments and the material interface between the 4th and 5th slit depth is given by

$$\mathbf{C} = \left[\begin{array}{cccc|cccc} 0 & 0 & 0 & 0 & 0 & 0 & 0 & 0 \\ -1 & 2 & -1 & 0 & 0 & 0 & 0 & 0 \\ 0 & -1 & 2 & -1 & 0 & 0 & 0 & 0 \\ 0 & 0 & 0 & 0 & 0 & 0 & 0 & 0 \\ 0 & 0 & 0 & 0 & 0 & 0 & 0 & 0 \\ 0 & 0 & 0 & 0 & -1 & 2 & -1 & 0 \\ 0 & 0 & 0 & 0 & 0 & -1 & 2 & -1 \\ 0 & 0 & 0 & 0 & 0 & 0 & 0 & 0 \end{array}\right], \boldsymbol{\sigma} = \left\{\begin{array}{c} \sigma_1^A \\ \sigma_2^A \\ \sigma_3^A \\ \sigma_4^A \\ \sigma_5^B \\ \sigma_6^B \\ \sigma_7^B \\ \sigma_8^B \end{array}\right\} \quad (4)$$

where σ_i^A, refers to the stress over depth increment *i* where that increment is in material A as compared to material B. For visual illustration, lines are shown in Eq. 4 to indicate the material interface where a stress discontinuity is allowed. Note that none of the (-1 2 –1) patterns in **C** cross the interface.

Further pairs of rows can be removed for additional interfaces. If the location of an interface is not known with sufficient precision, more than two rows may need to be removed to ensure the discontinuity is resolved.

Calibration coefficients

The calibration coefficients (**G** in Eqs. 1 and 2) are calculated using a finite element model, which is standard practice for the slitting method [18,19]. The calculation must model all *n* slit depths, and the *i*th slit depth must calculate a coefficient for *i* pulse loads, making for *n*(n-1)/2* calculations. In this work, the Abaqus software [20] was used along with the Python scripting interface, which allows for automation of the multiple calculations.

EXPERIMENTAL

Aluminum clad depleted-uranium fuel plates

The purpose of the Department of Energy- National Nuclear Security Administration's Global Threat Reduction Initiative's (GTRI) Reactor Conversion program, formerly known as the Reduced Enrichment for Research and Test Reactors (RERTR) program, is to work with research reactor operators worldwide in an effort to convert reactors from the use of highly enriched uranium (HEU) fuel to the use of low enriched uranium (LEU). In support

of this effort, the Reactor Conversion program is working to develop new fuels to allow for the conversion of high performance research reactors worldwide. A significant goal for GTRI's Reactor Conversion program is converting high performance research reactors from highly enriched uranium (HEU) dispersion fuel plates to low enriched uranium (LEU) monolithic fuel plates. This requires development, qualification, and production of high-density, monolithic LEU-10Mo (wt. pct.) foils [21]. The monolithic fuel foils are to be co-rolled with Zr and clad with 6061Al using hot isostatic pressing (HIP) [22].

For testing purposes, samples were prepared using Depleted Uranium (DU) instead of LEU. Through-thickness profiles of the longitudinal residual stress were measured in two clad fuel plates with DU-10Mo elements, coated with a 20 μm zirconium layer, sandwiched between layers of Al 6061. Both samples were slit using wire Electric Discharge Machining (wire EDM) with a 100 μm diameter brass wire, and strain gages (two for redundancy) on the back face opposite the cut. One plate had 0.61 mm thick DU off-center in a 4.6 mm total plate thickness and was slit in increments of 50.8 μm. The other plate had 0.28 mm thick DU off-center in a 1.5 mm thick plate and was cut in increments of 25.4 μm. Figure 2 shows the test setup and the strain data.

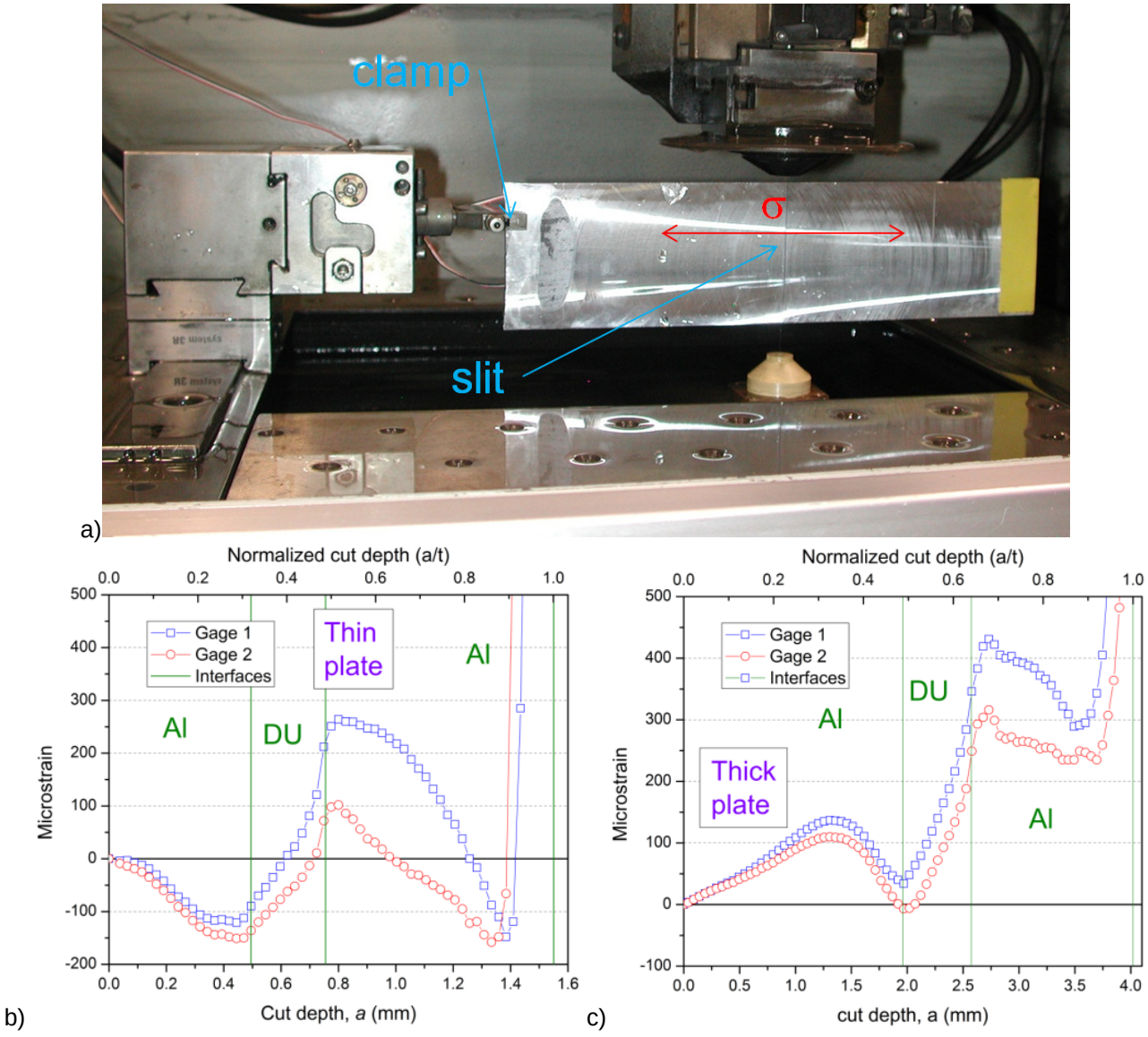

Figure 2. a) One of the plates in the EDM machine after slitting was completed. The strain gauges are on the opposite face. b) strain data on the thin plate and c) on the thick plate.

Multi-Layered Ceramic

As part of an effort to manufacture functionally graded ceramics and mesoscale heat exchangers [23-25], 18 mm diameter multi-layered disk were fabricated using novel powder processing and sintering technology. A slitting measurement was performed on a disk with a 0.875 mm thick alumina layer, a 0.835 mm thick mixed alumina-zirconia layer, and then a 0.943 mm thick layer of zirconia [26]. Here we present a re-analysis of the old data. Table 1 shows the elastic and thermal expansion properties of the materials.

Material	E	ν	α
Alumina	350 GPa	0.23	8.1×10^{-6}/C
Zirconia	200 GPa	0.3	10.3×10^{-6}/C
50/50	265 GPa	0.267	9.07×10^{-6}/C

Table 1. Material properties used to calculate calibration coefficients in finite element model.

Figure 3 shows the experimental setup. A grinding wheel was used to initially make a diametrical slit 25-μm deep. The diamond grinding wheel was 1.07-mm thick and 152.9-mm in diameter. The wheel was spinning at 3600 RPM, and approximately 1 μm was removed in each pass of the wheel while bathing the cut in coolant. A strain gage had been mounted on the circular face of the specimen opposite the cut to measure the strain in the direction normal to the slit face. A strain reading was taken after the cut. The slit was then deepened in increments of 25-μm, with a strain reading taken after each increment.

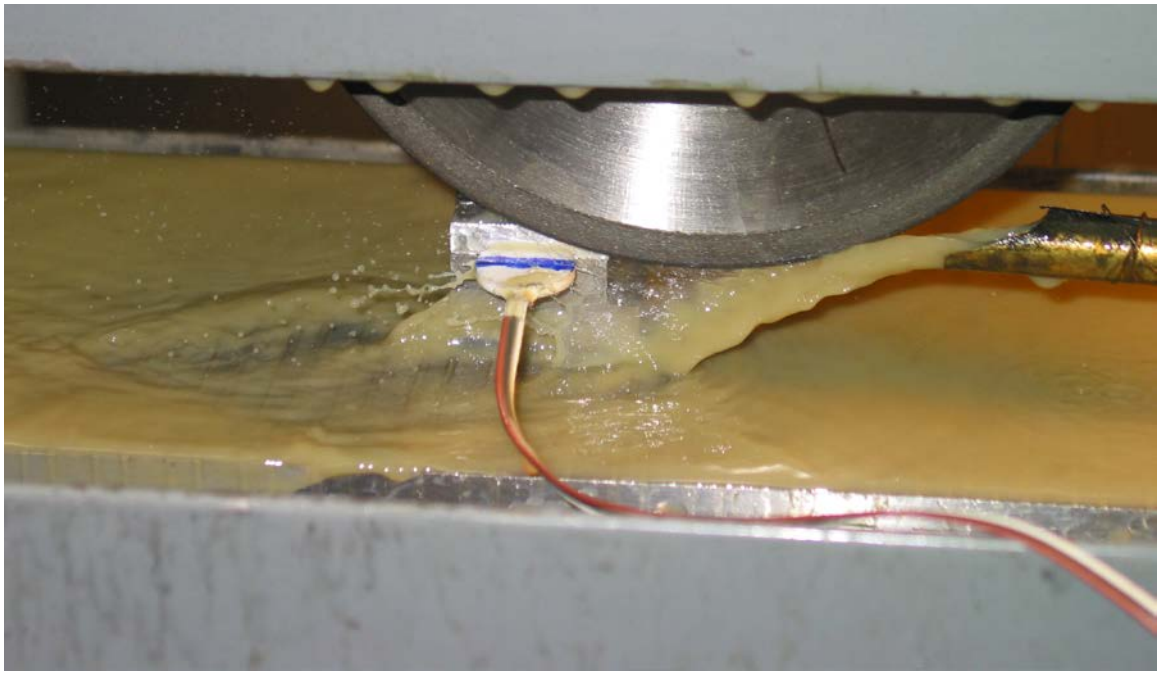

Figure 3. The test specimen during the slitting process.

The specimen was cut from the Alumina side to about 89% of the specimen thickness. Figure 4 shows the data. Because the specimen is curved from the same cooling deformations that cause the residual stresses, the strains are plotted versus an average slit depth

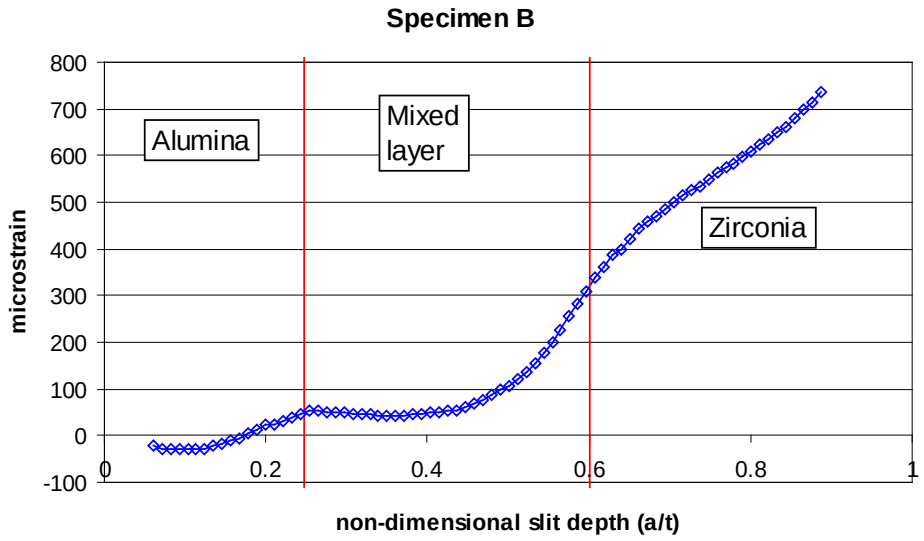

Figure 4. Data from second slitting test.

RESULTS

Aluminum clad depleted-uranium fuel plates

The calibration coefficients (**G** in Eqs. 1 and 2) were calculated using a 2-D, plane strain finite element model that included all the materials. The data was analyzed separately using the strain data from each gage as a check of repeatability. Figure 5 shows the resulting stress profiles. Although the locations of the thin zirconium layers are indicated, they were too small for their stresses to be independently identified by the measurements. The stress profiles show modest stress levels with significant discontinuities across the material interfaces. The stress magnitudes are generally limited by the yield strength of the 6061 Al which is reduced significantly because of the thermal history during the HIP process [27]. To aid interpreting the stresses, Figure 6 shows a model of the stress profile in the thinner plate based on thermal expansion mismatch and elasticity. Because the model was meant to be explanatory rather than predictive, the temperature change was adjusted down to 200 ºC (compared to HIP ΔT of ~530 ºC) in order to get similar stress magnitudes. The basic nature and slopes of the stress profiles in Figure 5 are well predicted by the thermal mismatch and the requirements of force and moment balance. The more complicated stress profile in the DU layer may come from residual stresses existing prior to the bonding process or from localized plasticity at the material interface.

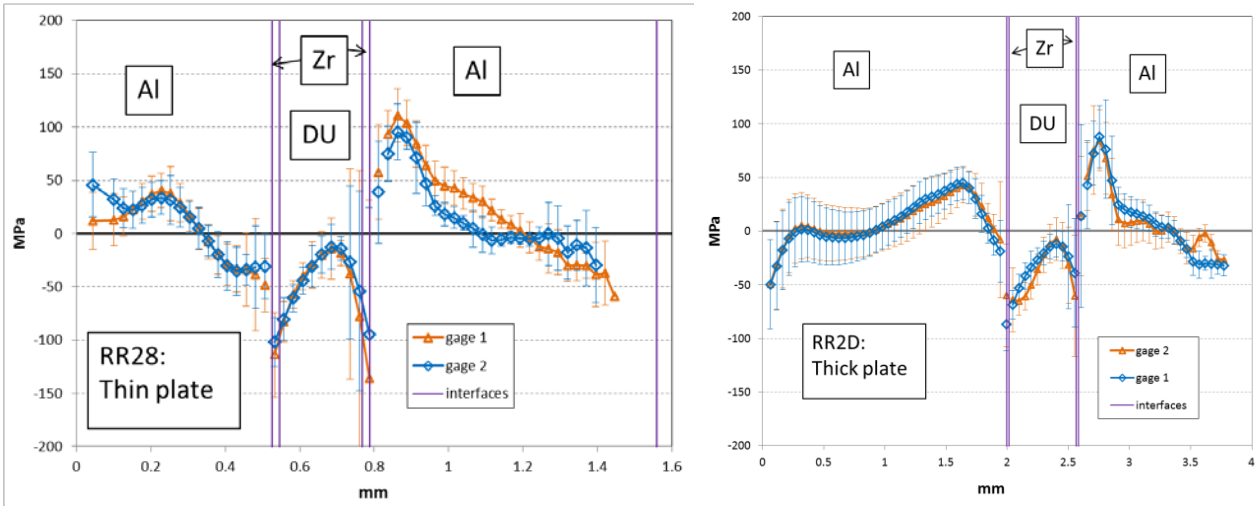

Figure 5. Through-thickness stress profiles in layered plates.

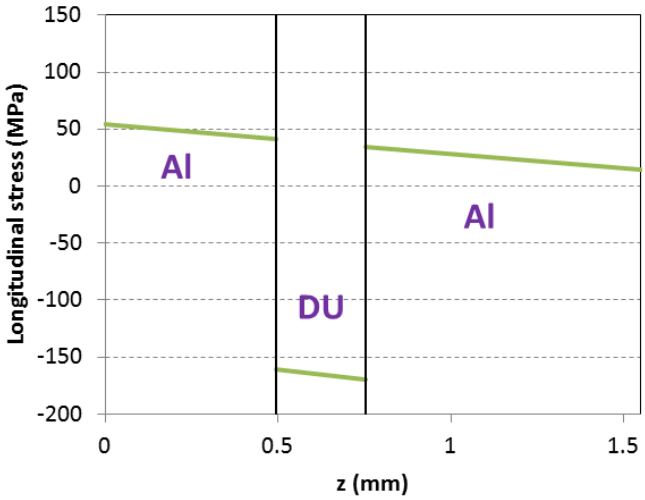

Figure 6. Prediction of stress profile in thinner plate based on thermal expansion mismatch and elasticity.

Figure 7 shows how well the inverse solution that gave the stresses in Figure 5 fits the data. The root-mean-square error for the fits ranges from about 1.5 to 2.5 με. Other inverse solutions, such as polynomial series, would not fit the data nearly so well.

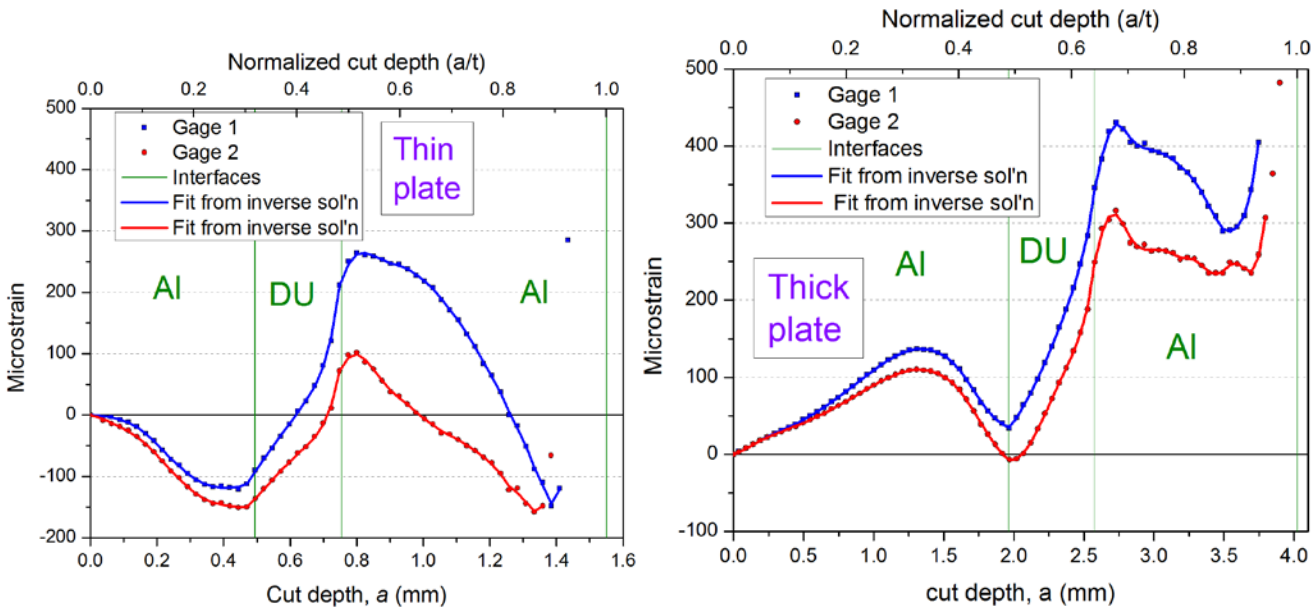

Figure 7. The strain fit given by the inverse solution matched the data much better than other inverse solutions.

Multi-Layered Ceramic

The calibration coefficients (**G** in Eqs. 1 and 2) were calculated using a 3-D, finite element model that included all the materials. Figure 8 shows the mesh. The mesh does not include the curvature of the actual specimen because of the difficulty of meshing the curved multi-layered part with the straight slits from the measurement.

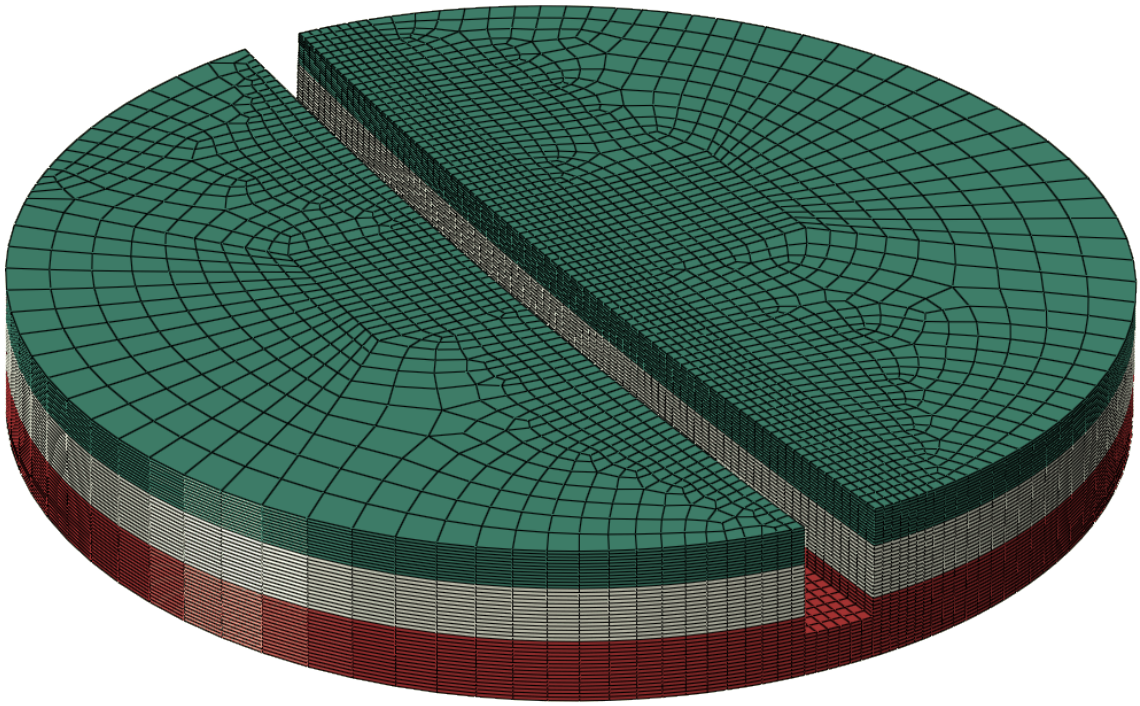

Figure 8. The finite element model used to calculate the calibration coefficients for the data reduction procedure. The model is shown in an intermediate step with the slit at partial depth.

The finite element model used coarser slit increments than the experiment. For simplicity of analysis, the strain data was interpolated to the depth increments from the model and analyzed. Because of the part curvature, the experimental slit did not simultaneously cross a material interface along the whole length of the slit. Rather, the crossing took several slit depth increments. This issue made the resolution of the stress discontinuities across the interfaces more difficult, and extra rows in the **C** matrix (eq. 4) were zeroed to allow the "discontinuity" to occur over two depth increments.

Figure 9 shows the through-thickness stress profile as determined by slitting measurements and the pulse-regularization method allowing for discontinuities. The stresses are significant and vary approximately linearly within each layer, with very large discontinuities across layers. A couple of stresses near the second interface appear as intermediate values, in the region were discontinuities were allowed. These points probably reflect the inability to resolve the discontinuity because of the non-uniform slit depth with respect to the interface boundary. For reference, Figure 9 also plots the results of a simple prediction of elastic, thermal-mismatch stresses using the properties from Table 1. The results agree quite well with the trends in the results, with the results for a temperature change of 900 °C agreeing somewhat better than the results for the actual temperature change of about 1200 °C.

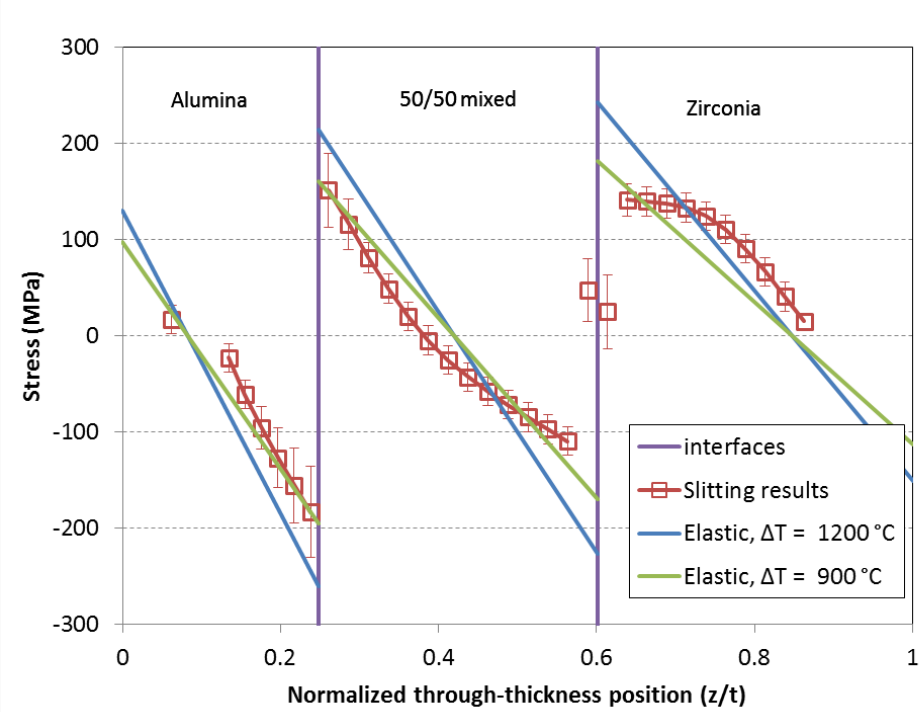

Figure 9. Through-thickness stresses measured in multi-layered ceramic, compared to elastic analysis of thermal mismatch stresses.

Figure 10 shows how well the inverse solution that gave the stresses in Figure 9 fits the data. The root-mean-square error for the fits ranges from about 4.8 με, with most of the misfit being evident for the data at shallow cut depths. A fairly large β (eq. 2) was used to force the results to stress profiles with less curvature in the regions away from the interfaces. The data for shallow slit depths is the most affected by the issue with part curvature, which is why more regularization was needed in order to reconcile the data with a smoother stress profile.

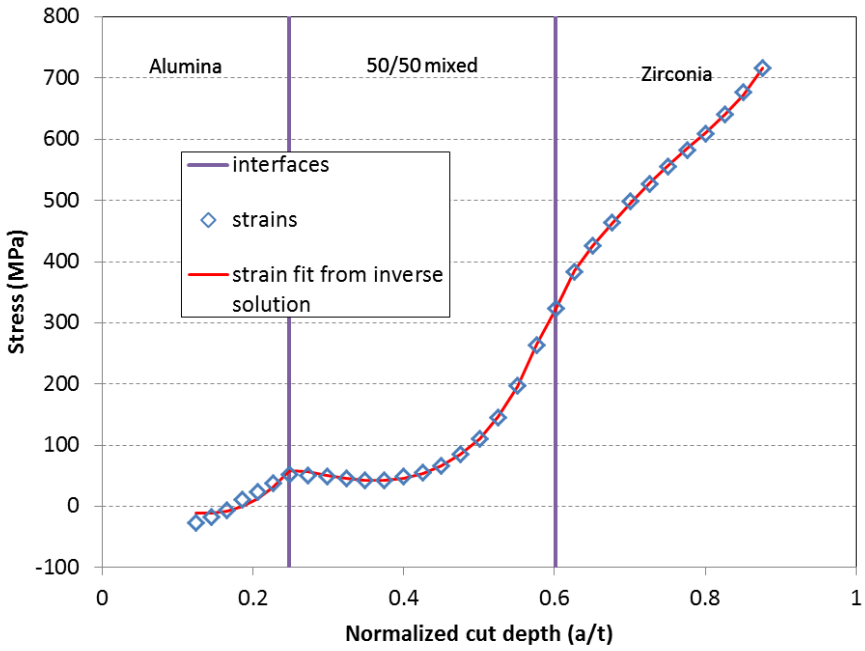

Figure 10. The strain fit given by the inverse solution matched the data quite well.

CONCLUSION

Residual stress profiles in layered samples were measured using the incremental slitting method. Using a modified pulse-regularization inverse solution approved to be superior to other approaches for solving the inverse problem because simultaneously:

1. It was able to resolve gradients in the residual stress profiles
2. It allowed for smoothing of the solution where appropriate while at the same time allowing for stress discontinuities across the layers
3. The resulting stress profiles were able to reproduce (i.e. fit) the measured strain data to within experimental accuracy.

With the power and flexibility of the modified pulse-regularization method, the ability to resolve discontinuous stress profiles for the tests in this paper was limited by experimental issues. In the aluminum clad depleted-uranium fuel plates, the plates were very wide and the layers were not of uniform thickness. In the multi-layered ceramic, the specimen was curved, but the slits were straight. So in each case, it was difficult to precisely know the slit depth relative to the interface location. For the fuel plates, it would have been possible to cut out a test specimen of thinner width without changing the longitudinal stresses, and then get a better controlled slit depth relative to the interface location. For the ceramic, we plan to test a new specimen with a symmetric layer arrangement and, therefore, no curvature.

ACKNOWLEDGEMENTS

This work was performed at Los Alamos National Laboratory, operated by the Los Alamos National Security, LLC for the National Nuclear Security Administration of the U.S. Department of Energy under contract DE-AC52-06NA25396. By acceptance of this article, the publisher recognizes that the U.S. Government retains a nonexclusive, royalty-free license to publish or reproduce the published form of this contribution, or to allow others to do so, for U.S. Government purposes. The authors would like to acknowledge the financial support of the US Department of Energy- National Nuclear Security Administration's Global Threat Reduction Initiative's Reactor Conversion program.

REFERENCES

1. Withers PJ (2007) Residual stress and its role in failure. Reports on Progress in Physics 70 (12):2211-2264
2. James MN (2011) Residual stress influences on structural reliability. Engineering Failure Analysis 18 (8):1909-1920
3. Cheng W, Finnie I (2007) Residual Stress Measurement and the Slitting Method. Mechanical Engineering Series Springer Science+Business Media, LLC, New York, NY, USA
4. Hill MR (2013) The Slitting Method. In: Schajer GS (ed) Practical Residual Stress Measurement Methods. John Wiley and Sons, Chichester, England,
5. Wong W, Hill MR (2012) Superposition and Destructive Residual Stress Measurements. Experimental Mechanics 53 (3):339-344. doi:10.1007/s11340-012-9636-y
6. Aydiner CC, Ustundag E, Prime MB, Peker A (2003) Modeling and measurement of residual stresses in a bulk metallic glass plate. Journal of Non-Crystalline Solids 316 (1):82-95
7. Prime MB, Hill MR (2004) Measurement of Fiber-Scale Residual Stress Variation in a Metal-Matrix Composite. Journal of Composite Materials 38 (23):2079-2095
8. Rankin JE, Hill MR (2003) Measurement of thickness-average residual stress near the edge of a thin laser peened strip. Journal of Engineering Materials and Technology 125 (3):283-293
9. Cheng W, Finnie I (1985) A method for measurement of axisymmetric axial residual stresses in circumferentially welded thin-walled cylinders. Journal of Engineering Materials and Technology 107 (3):181-185
10. Gremaud M, Cheng W, Finnie I, Prime MB (1994) The compliance method for measurement of near surface residual stresses-analytical background. Journal of Engineering Materials and Technology 116 (4):550-555
11. Cheng W, Finnie I, Gremaud M, Rosselet A, Streit RD (1994) The compliance method for measurement of near surface residual stresses-application and validation for surface treatment by laser and shot-peening. Journal of Engineering Materials and Technology 116 (4):556-560
12. Finnie S, Cheng W, Finnie I, Drezet JM, Gremaud M (2003) The computation and measurement of residual stresses in laser deposited layers. Journal of Engineering Materials and Technology 125 (3):302-308
13. Ersoy N, Vardar O (2000) Measurement of residual stresses in layered composites by compliance method. Journal of Composite Materials 34 (7):575-598
14. Schajer GS, Prime MB (2006) Use of Inverse Solutions for Residual Stress Measurements. Journal of Engineering Materials and Technology 128:375-382
15. Hill MR, VanDalen JE, Prime MB (2011) Assessment of Residual Stress in Fracture Mechanics Coupons. Paper presented at the ASME Conference Proceedings, doi:10.1115/PVP2011-57768
16. Schajer GS (1988) Measurement of non-uniform residual-stresses using the hole-drilling method .1. Stress calculation procedures. Journal of Engineering Materials and Technology 110 (4):338-343
17. Tikhonov AN, Goncharsky A, Stepanov V, Yagola AG (1995) Numerical methods for the solution of ill-posed problems, vol 328. Springer,
18. Lee MJ, Hill MR (2007) Effect of strain gage length when determining residual stress by slitting. Journal of Engineering Materials and Technology 129 (1):143-150
19. Rankin JE, Hill MR, Hackel LA (2003) The effects of process variations on residual stress in laser peened 7049 T73 aluminum alloy. Materials Science & Engineering A A349 (1/2):279-291
20. Simulia Abaqus 5.12-1 (2012). Dassualt Systems.,
21. Wachs DM, Clark CR, Dunavant RJ (2008) Conceptual Process Description for the Manufacture of Low-Enriched Uranium-Molybdenum Fuel.
22. Crapps J, Clarke K, Katz J, Alexander DJ, Aikin B, Vargas VD, Montalvo JD, Dombrowski DE, Mihaila B (2013) Development of the hot isostatic press manufacturing process for monolithic nuclear fuel. Nuclear Engineering and Design 254:43-52
23. Shin H, Case E, Kwon P (2003) Fabrication of internal channels in ceramics and ceramic composites. Journal of advanced materials 35 (2):28-35
24. Case ED, Ren F, Kwon P, Kok CK, Rachedi R, Klenow B (2005) Machining and Ceramic/Ceramic Joining to Form Internal Mesoscale Channels. International Journal of Applied Ceramic Technology 1 (1):95-103
25. Sun L, Kwon P (2010) ZrW2O8–ZrO2 Continuous Functionally Graded Materials Fabricated by In Situ Reaction of ZrO2 and WO3. Journal of the American Ceramic Society 93 (3):703-708
26. Ekbote B, Kwon P, Prime MB Micromechanics-based Design and Processing of Efficient Meso-scale Heat Exchanger. In: Mallick PK (ed) Proceedings of the American Society for Composites - 21st Technical Conference, Dearborn , MI., 2006.
27. Alexander DJ, Clarke KD, Liu C, Lovato ML (2011) Tensile Properties of 6061 Aluminum Alloy Materials. Los Alamos National LAboratory report LA-UR-11-06707